Morphological Control and Luminescent Properties of YVO_4:Eu Nanocrystals

Xingcai Wu,* Yourong Tao, Chunyan Song, Changjie Mao, Lin Dong, and Junjie Zhu

Key Laboratory of Mesoscopic Chemistry of MOE, the State Key Laboratory of Coordination Chemistry, and School of Chemistry and Chemical Engineering, Nanjing University, Nanjing 210093, P. R. China

Received: January 25, 2006; In Final Form: June 22, 2006

Rodlike, olivelike, pineapplelike, and particlelike nanocrystals of theYVO_4:Eu (5 at. % Eu) were synthesized by a hydrothermal reaction with different conditions, respectively. The rodlike nanocrystal has a rectangular cross-section with about 35×60 nm^2 and a length of about 220 nm. The olivelike nanocrystal has an equatorial diameter of ∼40 nm and a length of ∼200 nm. The pineapplelike nanocrystal with an equatorial diameter of ∼200 nm and a length of ∼300 nm, is a superstructure consisting of self-organized nanorods with a diameter of ∼20 nm and a length of ∼50 nm. The particlelike nanocrystals show globular and polyhedral shape with a diameter of ∼50 nm. Their UV−vis absorption peaks are at 305, 308, 285, and 280 nm, respectively, and there is such a trend that the absorption peaks shift to higher energy as the size of the particles decreases. Compared with other-shape nanocrystals, the luminescence intensity of the olivelike nanocrystals is obviously enhanced. It suggests that we could obtain the function-improved materials by tailoring the size and shape of theYVO_4:Eu nanostructures.

Introduction

Yttrium orthovanadate (YVO_4) is an important oxide in materials science and technology, for example, its large single crystal has been extensively used as an excellent polarizer[1,2] and laser host material,[3,4] whereas its powder doped Eu^{3+} has been used as a red phosphor in color television and cathode ray tubes (CRTs)[5,6] owing to its high luminescence efficiency upon electron-beam excitation. Studies still show that YVO_4: Nd crystal serves as a matrix for diode-pumped solid state lasers, and the absorption coefficient at 808 nm, which is the standard wavelength of currently available laser diodes, is five times the one in YAG: Nd,[7] and bulk YVO_4:Eu has a high photoluminescent (PL) quantum yield of about 70%.[8] Bulk YVO_4: Eu can be prepared either by solid-state reaction at temperatures above 1300 K, or by solution chemistry method including hydrothermal synthesis,[9] hydrolyzed colloidal reaction (HCR) technique,[10] and induced precipitation.[11] YVO_4 single crystals have been grown using various techniques such as Czochralski (CZ),[12] top-seeded solution growth (TSSG),[13] floating zone (FZ),[14] and laser heated pedestal growth (LHPG).[15] YVO_4 thin films have been prepared by pulsed laser deposition (PLD),[16] chemical vapor deposition (CVD),[17] the hydrothermal electrochemical method, [18] sol−gel techniques,[19] and the microwave-assisted chemical solution deposition.[20] Compared with bulk materials, nanoscale materials have unique physical or chemical properties and applications,[21] so investigation into synthesis and luminescence property of YVO_4 nanocrystals doped with rare-earth ions is just beginning to emerge.[22] However, the morphological control of the YVO_4 nanocrystals is still a challenge, especially preparation of single-crystalline YVO_4 nanorods. Wu et al. once tailored the size and shape of YVO_4 crystallites by changing the reaction condition such as yttrium-to-vanadium ratio, pH value, reaction temperature and time, and organic molecules additives (ethylenediaminetetraacetic acid, acetic acid, and ethanol),[23] but only obtained YVO_4 nanograins and nanoflakes, and did not concern their physical or chemical properties. Recently, Chen et al.[24] have reported morphological control of YVO_4:Eu nanocystallites by variation of the pH value (8−14) in the basic solution, and pointed out that luminescence intensity increased from bundle-like, rice-like to rhombus-like nanocrystals. It is an interesting result, but it lacks detail microstructure characterization and ultraviolet−visible (UV−vis) data of the nanostructures. We once prepared single-crystal $NdVO_4$ nanorods [25] and polycrystalline YVO_4 nanorods and microtubes[26] by using $(NH_4)_{0.5}V_2O_5$ nanowires templates.[27] Here, we describe the controlled growth of rodlike, olivelike, and pineapplelike nanocrystals of the YVO_4:Eu by using porous silicon substrates, V_2O_5 nanowires, and CTAB (cetyltrimethylammonium bromide) additives at pH 6−7, respectively, and further investigate into their microstructure, luminescence, and UV−vis absorption properties. For comparison, the dispersed nanoparticles of the YVO_4:Eu were also prepared.

Experimental Section

Preparation of the Samples. *Rodlike YVO_4:Eu Nanocrystals (sample 1).* In a typical synthesis, 124.6 mg of Y_2O_3 and 10.2 mg of Eu_2O_3 were heated to dissolve in 5 mL of 1:1 nitric acid, and adjusted to a pH value of about 6−7 with 1:1 $NH_3 \cdot H_2O$. The suspension was added with 136.0 mg NH_4VO_3 powders and deionized water to 35 mL, and stirred for 10 min, then transferred to a 50 mL Teflon-lined stainless steel autoclave. Then, a few porous silicon substrates ($1 \times 0.5 \times 0.1$ cm^3, silicon substrates were hydrothermally treated in 30% HF solution for 5 h at 140 °C) were added to the autoclave and it was sealed and maintained at 170 °C for 58 h, then cooled to room temperature. Finally, the precipitates in the solution were filtered and washed with deionized water three times, meanwhile the porous silicon substrates were removed, and then the products were dried at 80 °C in air.

Olivelike YVO_4:Eu nanocrystals (sample 2). Uniform nanowires of $(NH_4)_{0.5}V_2O_5$ were synthesized using a previously

* To whom correspondence should be addressed. E-mail: wuxingca@netra.nju.edu.cn. Fax: +86-25-83317761.

10.1021/jp060527j CCC: $33.50 © 2006 American Chemical Society
Published on Web 07/26/2006

reported preparation procedure,[27] having a diameter ranging from 30 to 80 nm and a length up to 0.5 mm. Then the $(NH_4)_{0.5}V_2O_5$ nanowires were converted into V_2O_5 nanowires in air at 450 °C, and the size and shape of the nanowires remained. The preparation procedure was as follows: 189.1 mg of Y_2O_3 and 15.5 mg of Eu_2O_3 were heated to dissolve in 5 mL of 1:1 nitric acid, and adjusted to a pH value of about 6−7 with 1:1 $NH_3 \cdot H_2O$. To the suspension was added 160.4 mg of V_2O_5 nanowires and 35 mL of deionized water, and stirred for 10 min, then transferred to a 50 mL Teflon-lined stainless steel autoclave. The autoclave was sealed and maintained at 170 °C for 48 h, then cooled to room temperature. The products were then filtered, washed with deionized water, and dried at 80 °C in air.

Pineapplelike YVO_4:Eu Nanocrystals (sample 3). The preparation procedure and the reagent quantities of sample 3 were the same as that of sample 1, but 200.0 mg CTAB was added to the reaction solution. It did not contain porous silicon substrates, and the pH of the solution was adjusted to 6−7, and the reaction remained for 26 h.

YVO_4:Eu Particlelike Nanocrystals (sample 4). The preparation procedure and the reagent quantities were the same as that of sample 1, but did not contain porous silicon substrates, and the reaction remained for 48 h.

Characterization Techniques. The products were characterized by an X-ray diffraction (XRD; Philips X'pert) with graphite monochromatized Cu K α-radiation, transmission electron microscope (TEM; JEOL-JEM 200CX), high-resolution electron microscopy with a point resolution of 0.19 nm (HRTEM; JEOL model JEM-2100), and scanning electron microscope (SEM; LEO-1530VP) with the selected area energy dispersive spectrometry (EDS). Ultraviolet−visible (UV−vis) absorption spectra of the suspensions with the same concentration were measured with a Lambda 35 spectrometer (Perkin-Elmer). Photoluminescence (PL) spectra were recorded on an Aminco Bowman series 2 luminescence spectrometer equipped with 150 W Xe-arc lamp at room temperature (SLM Inc.), and for comparison of the different samples, the emission spectra were measured with the same instrument parameters (8.0 nm for split width of excitation light, 4.0 nm for split width of emission light, and 660 V for PMT voltage). Infrared (IR) spectra of the samples were recorded on BRUKER VECTOR 22 infrared spectrometer using KBr technique.

Results and Discussion

Structure and Morphology. XRD patterns of samples 1−4 correspond, respectively, to Figure 1a−d, which can be indexed as a pure tetragonal phase (wakefieldite), approaching the standard values for the bulk YVO_4 ($a = 7.119$ Å and $c = 6.289$ Å; JCPDS no. 17-341). The least-squares refined crystallographic unit cell parameters are shown in Table 1. A trend of increasing cell volumes could be clearly observed as the particle size decreased. Decrease of the cell volume for sample 3 may be assigned to CTAB additives. Figure 2 indicates SEM images of samples 1−4, respectively. Figure 2a shows that sample 1 is composed of nanorods and nanoparticles, and the nanorods occupy about 80%. A typical nanorod has a rectangular cross-section with about 35×60 nm^2 and a length of about 220 nm. Figure 2b indicates the olivelike morphology of sample 2, with a diameter of ∼40 nm and a length of ∼200 nm, approaching the size of the nanorods in sample 1. Figure 2c displays that sample 3 has the pineapplelike morphology with an equatorial diameter of ∼200 nm and a length of ∼300 nm. Figure 2d reveals that sample 4 is a few irregular nanoparticles with a diameter of ∼50 nm.

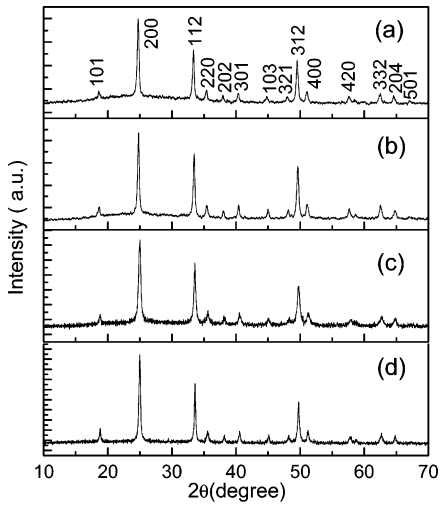

Figure 1. XRD patterns of the rodlike (a), olivelike (b), pineapplelike (c), and particlelike (d) nanocrystals of theYVO_4:Eu.

TABLE 1: Least-Squares Refined Unit Cell Parameters for $Y_{0.95}$ $Eu_{0.05}$ VO_4 Nanocrystalline Samples

no. of samples	a (Å)	c (Å)	error	$V = a^2c$ (Å^3)
JCPDS 17−341	7.119	6.289		318.7
sample 1 (rodlike)	7.1217	6.2923	±0.0002	319.14±0.028
sample 2 (olivelike)	7.1345	6.2799	±0.0002	319.65±0.028
sample 3 (pineapplelike)	7.1187	6.2778	±0.0002	318.13±0.028
sample 4 (particlelike)	7.1430	6.2942	±0.0002	321.15±0.028

TEM images of samples 1−4 are shown as Figure 3a−d, respectively, whereas HRTEM images and selected area electron diffraction (SAED) patterns of a single nanoparticle corresponding to samples 1−4 are revealed in Figure 3e−h, respectively. Figure 3a further confirms rodlike shape of sample 1, whereas HRTEM image and SAED pattern (inset) of a single nanorod show that they are single crystalline. HRTEM fringe spaces with 0.36 and 0.47 nm correspond to the 200 and 101 planes of theYVO_4, respectively. Based on the analysis of the HRTEM image and SAED pattern (inset right and below), the crystal structure of the nanorod was drawn on the right and above inset in Figure 3e. The nanorod grows along the 002 direction. TEM image in Figure 3b reveals an olivelike shape and rough surface of sample 2, whereas HRTEM image and SAED pattern of a single nanoparticle of sample 2 (Figure 3f) shows that it still is single crystalline, and grows along the 002 direction. Figure 3c is TEM image of sample 3, indicating the pineapplelike morphology, and the pineapplelike nanocrystals consist of self-organized single-crystalline nanorods with a diameter of about 20 nm and a length of about 50 nm. SAED pattern of a single pineapplelike nanoparticle (inset in Figure 3c) also shows that the nanoparticle is a polycrystalline superstructure. HRTEM image (Figure 3g) reveals bend of fringe, and particle edges, while fringe spacing with 0.35 nm shows the 200 plane of the nanoparticle. Figure 3d displays a few dispersed nanoparticles of sample 4, and there is either globular or polyhedral shape. HRTEM image of a typical nanoparticle is revealed as Figure 3h, and the shape approaches the nanorod of sample 1, but the ratio of length and diameter is smaller, so they probably have similar growth mechanism.

Morphological Control. Formation of YVO_4 nanocrystals is not only related to the pH value of the solution, but also to the concentration of Y^{3+} and VO_3^- (or VO_4^{3-}). When reagent concentration is high (e.g., about 0.2 mol·L^{-1}), a pure YVO_4 phase can form in strong basic solution (pH > 12). Under the

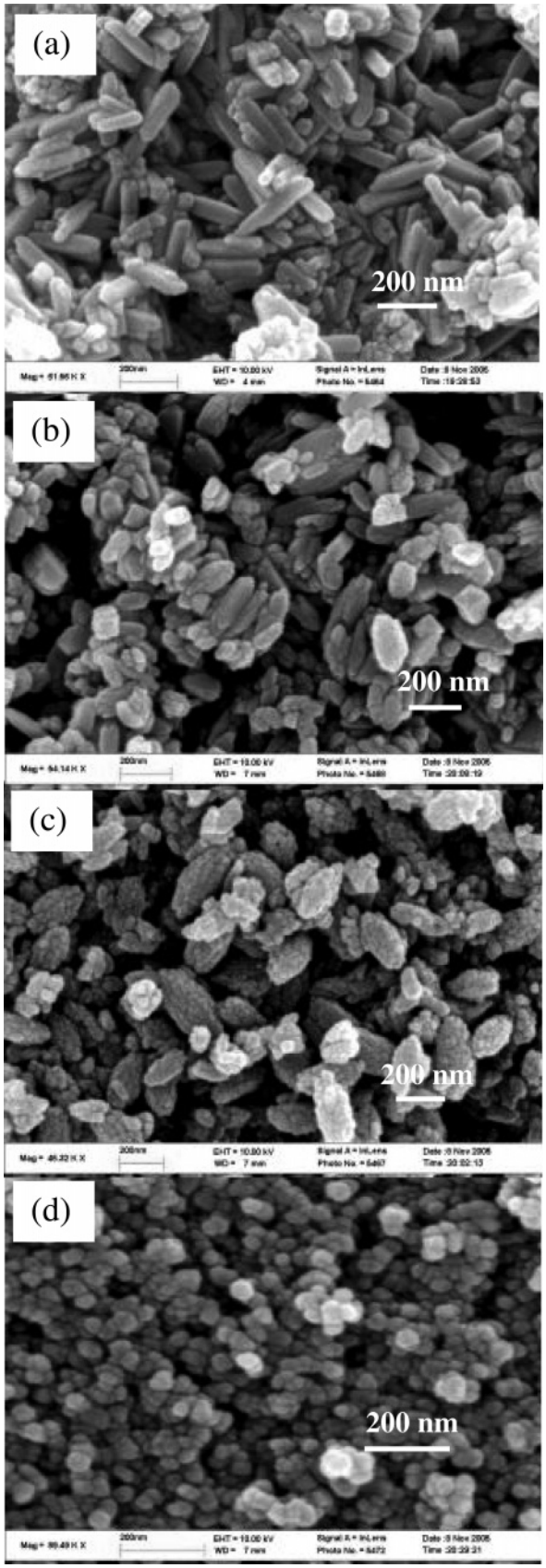

Figure 2. SEM images of the rodlike (a), olivelike (b), pineapplelike (c), and particlelike (d) nanocrystals of theYVO_4:Eu.

condition of present concentration, if the pH value of the solution is greater than 12, final products are only $Y(OH)_3$. If the pH is less than 2, V_2O_5 nanowires are formed, so an optimal pH is confirmed as about 5−7.

To get YVO_4:Eu nanorods, poly(ethylene glycol) 20000 or 600 was once selected as template agents, but only YVO_4:Eu nanoparticles were obtained. When porous silicon substrates were added to solution, a large number of short single-crystal nanorods were prepared (sample 1), or else, even if the reaction time was prolonged to 96 h according to the prepared condition of sample 1, the nanorods could not yet be obtained. Therefore, the porous silicon plays an important role in formation of theYVO_4:Eu nanorods. It is possible that the defects on porous silicon provide the growth point of the heterogeneous nucleation to promote the growth of the nanorods, similar to formation of YVO_4:Eu films on porous silicon substrates.[20] Because the YVO_4:Eu nanorod has a sharp tip, a solid−liquid−solid (SLS) mechanism of top-growth can be suggested. When NH_4VO_3 was replaced with V_2O_5 nanowires, a large number of olivelike YVO_4:Eu nanoparticles (sample 2) could be obtained. Because the olivelike nanoparticles are single-crystalline short rods, and have two tips similar to ZnO nanorods prepared by hydrothermal method,[28] the growth process can be still explained by a SLS mechanism. Although the V_2O_5 nanowires do not play a template role, they slowly dissolve and keep low concentrations of VO_3^- (or VO_4^{3-}), so it is probably helpful for one-dimensional growth. Similarly, the SLS mechanism may also be used to explain the formation of samples 3 and 4. In fact, the SLS mechanism here is only a Ostwald ripening process.[28] In addition, sample 3 shows the formation of superstructures containing dispersed YVO_4:Eu nanoparticles, similar to self-organized Ruthenium nanoparticles prepared by ion liquid,[29] so the CTAB probably plays a template role in the formation of the superstructure. Certainly, the actual growth mechanism of these nanostructures should be further investigated.

UV−Vis Absorption Spectra. Figure 4 shows the UV−vis absorption spectra of the sample suspension with 4.6×10^{-4} mol·L^{-1} (the suspensions were dispersed with an ultrasonic bath before they were measured). As Figure 4 shows, the absorption peaks of samples 1−4 are at 305, 308, 285, and 280 nm, respectively. It is reported that the UV−vis absorption (λ_{max} = 272 nm) of the YVO_4:Eu nanoparticles (in sizes ranging from 10 to 30 nm) does not significantly differ from that (λ_{max} = 267 nm) isolated by vanadate ions dissolved in solution,[22a] and the absorption peak can be assigned into the $^1A_1 \rightarrow {}^1T_1$ ($t_1 \rightarrow$ 2e) transition of the VO_4^{3-} ion. Generally, the $^1A_1 \rightarrow {}^1T_1$ ($t_1 \rightarrow$ 2e) transition is forbidden, as the size of the particles decreases and the deformation of the structure increases, $^1A_1 \rightarrow {}^1T_1$ transition can be partly allowed.[30] However, in our experiment, there is such a trend that the absorption peaks shift to higher energy as the size of the particles decreases, and absorption energy of all samples is lower than that of the reported YVO_4:Eu nanoparticles (in a size range of 10−30 nm). It may be explained by quantum confinement effects, [31] i.e., as the size of the ultrafine particles decreases, the energy gap widens so that the absorption peaks shift to higher energy.

Photoluminescence. Photoluminescence (PL) spectra of the sample suspension with 4.6×10^{-4} mol·L^{-1} (the suspensions were dispersed with an ultrasonic bath before they were measured) were recorded by a fluorescence spectrometer at room temperature. Figure 5 a−d shows photoluminescence excitation spectra of the $Y_{0.95}Eu_{0.05}VO_4$ nanocrystals of samples 1−4 under the emission of 618 nm, respectively. All the samples have two excitation peaks at 307 and 328 nm, and the peak at 328 nm is stronger than the one at 307 nm for samples 1 and 2; however, the peak at 328 nm is slightly weaker than the one at 307 nm for sample 3. Furthermore, the peak at 328 nm is obviously weaker than the one at 307 nm for sample 4. Figure 6a−d shows

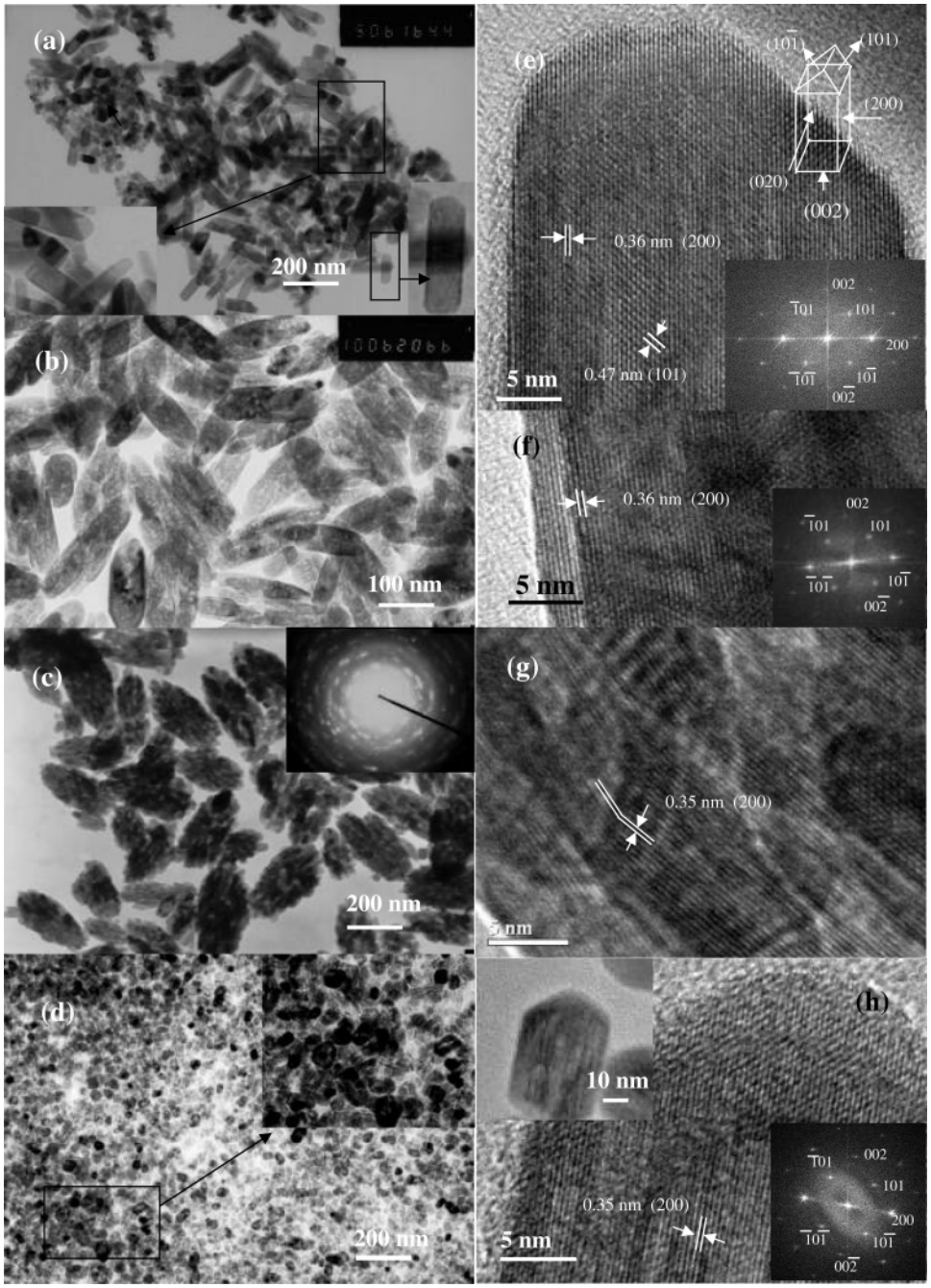

Figure 3. TEM image of the rodlike (a), olivelike (b), pineapplelike (c), and particlelike (d) nanocrystals of theYVO_4:Eu. HRTEM images and SAED patterns of the rodlike (e), olivelike (f), pineapplelike (g), and particlelike (h) nanocrystals of the YVO_4:Eu.

photoluminescence emission spectra of samples 1−4 under the excitation of 328 nm, respectively. The intense transitions observed in the luminescence spectrum originate from the $^5D_0$ level that is not split by the crystal field ($J = 0$). The peaks at 593, 618, 652, and 698 nm can be attributed to electric dipole transitions from the $^5D_0$ level to sublevel of $^7F_1$, $^7F_2$, $^7F_3$, and $^7F_4$, respectively, whereas the weak peak at 537 nm can be attributed to transition from $^5D_1$ to $^7F_1$.[5] Similar PL spectra can be obtained under the excitation of 307 nm. Whether the samples are excited at 328 or 307 nm, the emission of sample 2 obviously increases, and the emission of sample 3 decreases. As for sample 4, the peak at 618 nm is obviously stronger than the peak at 615 nm, which may be caused by the change of symmetry of the crystal fields around Eu^{3+} ions. Yan et al. once reported that the PL spectra of YBO_3:Eu nanocrystals showed a size-dependent characteristic which the ratio of the red emission transition ($^5D_0 \rightarrow {}^7F_2$) to the orange emission transition ($^5D_0 \rightarrow {}^7F_1$) was much higher in the smaller particles;[32] however, the effect is not obvious in our experiment since the ratios of the $^5D_0 \rightarrow {}^7F_2$ and $^5D_0 \rightarrow {}^7F_1$ integrated transition intensities are nearly the same in all samples (about 9.5). An important source of luminescence quenching in small particles is the surface where the coordination of the atom differs from that in the bulk and where different chemical species can be adsorbed. Because the samples were prepared in water, the surface of the nanocrystals can be covered with hydroxyl species such as yttrium or europium hydroxides, bending vanadates, additives, and the adsorbed water molecules. Because the PL of the samples is measured in suspension, the surface OH groups are efficient quenchers of the excited europium ions.[22c] Different size and shapes result in different combinative abilities between the surface and the adsorbed species so as to produce the

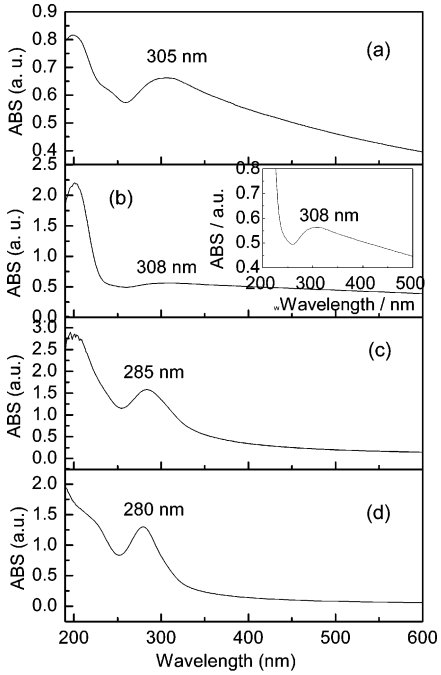

Figure 4. UV-vis absorption spectra of the rodlike (a), olivelike (b), pineapplelike (c), and particlelike (d) nanocrystals of theYVO_4:Eu.

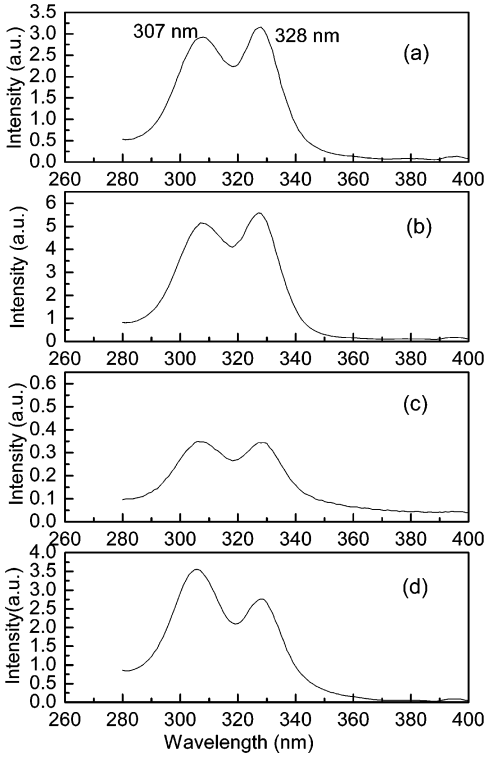

Figure 5. Photoluminescence excitation spectra of the rodlike (a), olivelike (b), pineapplelike (c), and particlelike (d) nanocrystals of the $Y_{0.95}Eu_{0.05}VO_4$ under the emission of 618 nm at room temperature.

different quenching abilities to the emission from Eu^{3+} ions, therefore, differences of PL intensity of the samples may be attributed into the different quenching abilities of the adsorbed species on the surface to the emission from Eu^{3+} ions. The luminescence intensity of the olivelike nanocrystals is obviously stronger than other samples, which may be because the nanostructures can prevent the adsorbed species on the surface from quenching the emission from Eu^{3+} ions. The IR spectra of the rodlike, olivelike, pineapplelike, and particlelike nano-

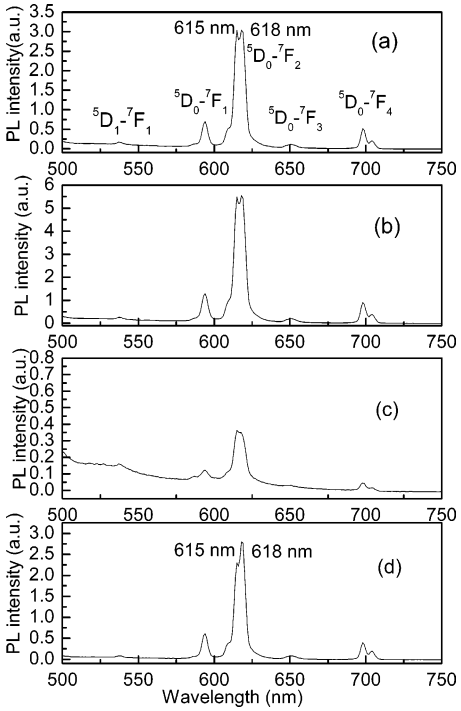

Figure 6. Photoluminescence emission spectra of the rodlike (a), olivelike (b), pineapplelike (c), and particlelike (d) nanocrystals of the$Y_{0.95}Eu_{0.05}VO_4$ under the excitation of 328 nm at room temperature.

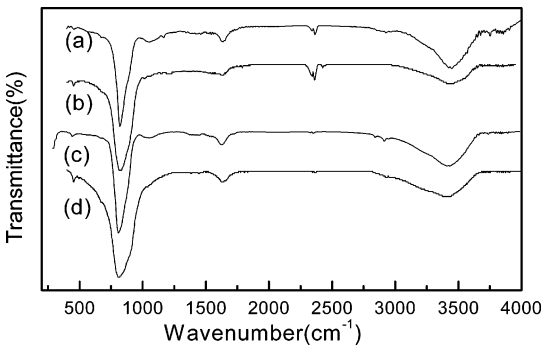

Figure 7. Infrared spectra of the rodlike (a), olivelike (b), pineapplelike (c), and particlelike (d) nanocrystals of the$Y_{0.95}Eu_{0.05}VO_4$.

crystals of the $Y_{0.95}Eu_{0.05}VO_4$ are, respectively, shown in parts a−d of Figure 7, similar to the reported IR spectra of $Y_{0.95}$-$Eu_{0.05}VO_4$.[22e,22f] As shown in Figure 7b for sample 2, a strong absorption peak at 823 cm^{-1} and a weak one at 456 cm^{-1} have appeared, which are attributed to the absorption of V−O and Y(Eu)-O bonds, respectively. A strong absorption peak at 3433 cm^{-1} and a weak one at 1629 cm^{-1} can be assigned into the symmetric stretching vibration and bending vibration of H−O−H (H_2O molecules), respectively. An absorption weak peak at 2358 cm^{-1} can be assigned into asymmetric stretching vibration of O═C═O (CO_2 molecules). In Figure 7c for sample 3, a peak at 2925 cm^{-1} could be observed obviously, which may be attributed to the stretching vibration of C−H bonds of CTA^+. Therefore, the luminescence quenching of sample 3 may be assigned into both species on the surface of the sample such as CTA^+ and OH groups.

Conclusion

In summary, single-crystal and olivelike nanorods of the YVO_4:Eu have been prepared by using porous silicon templates

and V_2O_5 nanowires, respectively. The pineapplelike and particlelike nanocrystals of the YVO_4:Eu have been synthesized with and without CTAB inducers, respectively. There is the obvious dependence of the UV−vis absorption on the particle size. Changes of PL intensity of the samples may be attributed into those of the quenching ability of the adsorbed species on the surface to the emission of Eu^{3+} ions.

Acknowledgment. The project was supported by Nanjing University Talent Development Foundation and the National Key Project for High-Tech. (no. 2003AA302150).

References and Notes

(1) Maunders, E. A.; Deshaser, E. G. *J. Opt. Soc. Am.* **1971**, *61*, 68.
(2) Ross, M. *IEEE J. Quantum Electron* **1975**, *11*, 938.
(3) O'Connor, J. R. *Appl. Phys. Lett.* **1966**, *9*, 407.
(4) Fields, R. A.; Birnbaum, M.; Fincher, C. L. *Appl. Phys. Lett.* **1987**, *51*, 1885.
(5) Levine, A. K.; Palilla, F. C. *Appl. Phys. Lett.* **1964**, *5*, 118.
(6) Levine, A. K.; Papilla, F. C. *Electrochem. Technol.* **1966**, *4*, 16.
(7) Barnes, N. P.; Storm, M. E.; Cross, P. L.; Skolant, M. W. *IEEE J. Quantum Electron* **1990**, *26*, 588.
(8) Wanmaker, W. L.; Bril, A.; ter Vrugt, J. W.; Broos, J. *Philips Res. Rep.* **1966**, *21*, 270.
(9) Nakhodnova, A. P.; Zaslavskaya, L. V. *Russ. J. Inorg. Chem.***1984**, *29* (6), 835. (b) Nakhodnova, A. P.; Zaslavskaya, L. V.; Pitsyuga, V. G. *Russ. J. Inorg. Chem.***1983**, *28* (3), 358. (c) Byrappa, K.; Nirmala, B.; Yoshimura, M. *Mater. Sci. Forum* **1999**, 315−317, 506.
(10) Erdei, S.; Rodriguez, N. M.; Ainger, F. W.; White, W. B.; Ravichandran, D.; Cross, L. E. *J. Mater. Chem.* **1998**, *8*, 99.
(11) (a) Ropp, R. C.; Oakley, R. German Patent 2056172, 1971 (b) Ropp, R. C. U.S. Patent 3580861, 1971.
(12) (a) Kuwano, Y.; Saito, S.; *Laser Study* **1990**, *18*, 616. (b) Muto, K.; Awasu, K.; *Jpn. J. Appl. Phys.* **1969**, *8*, 1360.
(13) Erdei, S. *J. Cryst. Growth* **1993**, *134*, 1.
(14) (a) Zheng, H.; Yang, H. G.; Zhang, Y. Z.; Zhou, J. F.; Xia, H. C.; Wu, X.; Jiang, Y. D. *J. Cryst. Growth* **1996**, *160*, 136. (b) Shonai, T.; Higuchi, M.; Kodaira, K. *Mater. Res. Bull.* **2000**, *35*, 225. (c) Yan, X. L.; Wu, X.; Zhou, J. F.; Zhang, Z. G.; Wang, X. M.; Fu, P. M.; Jiang, Y. D. *J. Cryst. Growth* **2000**, *212*, 204.
(15) Ardila, D. R.; Camargo, A. S. S.; Andreeta, J. P.; Nunes, L. A. O. *J. Cryst. Growth* **2001**, *233*, 253.
(16) (a) Kang, W.; Park, J.; Kim, D. K.; Suh, K. S. *Bull. Korean Chem. Soc.* **2001**, *22*, 921. (b) Korzenski, M. B.; Lecoeur, Ph.; Mercey, B.; Raveau, B. *Chem. Mater.* **2001**, *13*, 1545.
(17) Bai, G. R.; Zhang, H.; Foster, C. M., *Thin Solid Films* **1998**, *321*, 115.
(18) Watanabe, T.; Cho, W. S.; Suchanek, W. L.; Endo, M.; Ikuma, Y.; Yoshimura, M. *Solid State Sci.* **2001**, *3*, 183.
(19) Hirano, S.I.; Yogo, T.; Kikuta, K. I.; Sakamoto, W.; Koganei, H. *J. Am. Ceram. Soc.* **1996,** *79*, 3041.
(20) Xu, H. Y.; Wang, H.; Jin, T. N.; Han, H. *Nanotechnology* **2005**, *16*, 65.
(21) (a) Adachi, M.; Murata, Y.; Harada, M. *Chem. Lett.* **2000**, *29*, 942. (b) Xia, Y.; Yang, P.; Sun, Y.; Wu, Y.; Mayers, B.; Gates, B.; Yin, Y.; Kim, F.; Yan, H. *Adv. Mater.* **2003**, *15*, 353. (c) Huang, M. H.; Mao, S.; Feick, H.; Yan, H.; Wu, Y.; Kind, H.; Weber, E.; Russo, R.; Yang, P. *Science* **2001**, *292*, 1898. (d) Comini, E.; Sberveglieri, G.; Pan, Z.; Wang, Z. *Appl. Phys. Lett.* **2002**, *81*, 1869.
(22) (a) Riwotzki, K.; Haase, M. *J. Phys. Chem. B* **1998**, *102*, 10129. (b) Buissette, V.; Huigard, A.; Gacoin, T.; Boilot, J. P.; Aschehoug, P.; Viana, B. *Surface Science* **2003**, *444*, 532−535. (c) Huignard, A.; Buissette, V.; Franville, A.; Gacoin, T.; Boilot, J. *J. Phys. Chem. B* **2003**, *107*, 6754. (d) Nazara, M.; Bukesov, S.; Jeon, D. Y.; Popovici, E. J.; Muresan, L.; Akmaeva, T. *Moldavian J. Phys. Sci.* **2003**, *2* (3−4), 311. (e) Huignard, A.;Buissette, V.; Laurent, G.; Gacoin, T.; Boilot, J. P. *Chem. Mater.* **2002**, *14*, 2264. (f) Yu, M.; Lin; J, Fang; J. *Chem. Mater.* **2005**, *17*, 1783.
(23) Wu, H.; Xu, H.; Su, Q.; Chen, T.; Wu, M. *J. Mater. Chem.* **2003**, *13*, 1223.
(24) Chen, L.; Liu, Y.; Huang, K. *Mater. Res. Bull.* **2006**, *4*, 158.
(25) Wu, X. C.; Tao, Y. R.; Dong, L.; Zhu, J. J.; Hu, Z. *J. Phys. Chem. B* **2005**, *109* (23), 11544.
(26) Wu, X. C.; Tao, Y. R.; Mao, C. J.; Liu, D. J.; Mao, Y. Q. *J. Cryst. Growth* **2006**, *290*, 207.
(27) Wu, X. C.; Tao, Y. R.; Dong, L.; Hong, J. M. *J. Mater. Chem.* **2004**, *14*, 901.
(28) (a) Pacholski, C.; Kornowski, A.; Weller, H. *Angew. Chem., Int. Ed.* **2002**, *41*, 1188. (b) Cheng, B.; Samulski, E. T. *Chem. Commun.* **2004**, 986.
(29) Silveira, E. T.; Umpierre, A. P.; Rossi, L. M.; Machado, G.; Morais, J.; Soares, G. V.; Baumvol, I. J. R.; Teixeira, S. R.; Fichtner, P. F. P.; Dupont, J. *Chem. Eur. J.* **2004**, *10*, 3734.
(30) (a) Ronde, H.; Blasse, G. *J. Inorg. Nucl. Chem.* **1978**, *40*, 215. (b) Blasse, G. *Struct. Bonding* **1980**, *42*, 1.
(31) (a) Kubo, R. *J. Phys. Soc. Jpn.* **1962**, *17*, 975. (b) Mills, G.; Zongguan, L.; Meisel, D. *J. Phys. Chem.* **1988**, *92*, 822. (c) Brus, L. *J. Phys. Chem.* **1986**, *90*, 2555.
(32) Wei, Z.; Sun, L.; Liao, C.; Yin, J.; Jiang, X., Yan, C. *J. Phys. Chem. B* **2002**, *106*, 10610.